Where do Models go Wrong? Parameter-Space Saliency Maps for Explainability

Roman Levin *
Department of Applied Mathematics
University of Washington
rilevin@uw.edu

Manli Shu *
Department of Computer Science
University of Maryland
manlis@umd.edu

Eitan Borgnia *
Department of Computer Science
University of Maryland
eborgnia2@gmail.com

Furong Huang
Department of Computer Science
University of Maryland

Micah Goldblum
Department of Computer Science
University of Maryland

Tom Goldstein
Department of Computer Science
University of Maryland

Abstract

Conventional saliency maps highlight input features to which neural network predictions are highly sensitive. We take a different approach to saliency, in which we identify and analyze the network parameters, rather than inputs, which are responsible for erroneous decisions. We find that samples which cause similar parameters to malfunction are semantically similar. We also show that pruning the most salient parameters for a wrongly classified sample often improves model behavior. Furthermore, fine-tuning a small number of the most salient parameters on a single sample results in error correction on other samples that are misclassified for similar reasons. Based on our parameter saliency method, we also introduce an input-space saliency technique that reveals how image features cause specific network components to malfunction. Further, we rigorously validate the meaningfulness of our saliency maps on both the dataset and case-study levels.

1 Introduction

With the widespread deployment of deep neural networks in high-stakes applications such as medical imaging [13], credit score assessment [30], and facial recognition [7], practitioners need to understand why their models make the decisions they do. In fact, "right to explanation" legislation in the European Union and the United States dictates that relevant public and private organizations must be able to justify the decisions their algorithms make [28, 9]. Diagnosing the causes of system failures is particularly crucial for understanding the flaws and limitations of models we intend to employ.

Conventional saliency methods focus on highlighting sensitive pixels [23] or image regions that maximize specific activations [8]. However, such maps may not be useful in diagnosing undesirable model behaviors as they do not necessarily identify areas that specifically cause bad performance. The most sensitive pixels may not be the ones responsible for triggering misclassification, and may not be responsible for an observed high confidence score.

*Equal contribution

Preprint. Under review.

We develop an alternative approach to saliency that highlights network parameters that influence decisions rather than just input features. These maps yield a number of useful analyses:

- Nearest neighbors in parameter saliency space share common semantic information. Thus, if one image causes a network to malfunction, another image with a similar parameter saliency pattern is likely to suffer from a similar problem.
- By first identifying the network parameters responsible for a bad decision, we can then visualize the image regions that interact with those parameters and cause the identified misbehavior.
- Pruning the most salient network parameters for miss-classified images can improve model behavior on misclassified samples.
- Fine tuning a small number of salient filters on a single sample results in error correction on other samples that are misclassified for similar reasons.

After carefully delineating our methodology and experimentally validating the meaningfulness of our parameter saliency maps, we showcase the practical utility of this paradigm as an explainability tool with a case study in which we are able to uncover a neural network's reliance on a spurious correlation which causes interpretable failures. Our code for computing pararmeter saliency maps is available at https://github.com/LevinRoman/parameter-space-saliency.

1.1 Related work

Neural network interpretability and parameter importance. A major line of work in neural network interpretability focuses on convolutional neural networks. Works visualizing, interpreting, and analysing feature maps [32, 31, 18, 16] provide insight into the role of individual convolutional filters. These methods, together with other approaches for filter explainability [5] find that individual convolutional filters often are responsible for specific tasks such as edge, shape, and texture detection.

The idea of measuring neural network parameter importance has been studied in multiple contexts. Notions of neuron and parameter importance have been used for AI explainability [26, 19, 17, 21, 20], manipulating model behavior [4], and parameter pruning [1, 15].

Input space saliency maps. A considerable amount of literature focuses on identifying input features that are important for neural network decisions. These methods include using deconvolution approaches [32] and data gradient information [23]. Several works build on these ideas and propose improvements such as Integrated Gradients [27], SmoothGrad [24], and Guided Backpropagation [25] which result in sharper and more localized saliency maps. Other approaches focus on the use of class activation maps [33] with improvements incorporating gradient information [19] and more novel approaches to weighting the activation maps [29]. In addition, various saliency methods are based on manipulating the input image [10, 32]. Another line of work is aimed at evaluating the effectiveness of saliency maps [2, 3].

Although extensive work studies how different regions of *images* affect a network's predictions, limited work [26] aims to distinguish important network *parameters*. Our work combines the ideas of saliency maps and parameter importance and evaluates saliency directly on model parameters by aggregating their absolute gradients on a filter level, and we leverage the resulting saliency profiles as an explainability tool. We note that while existing input saliency maps used with the predicted label can highlight features that are related to misclassification, they do not shed light on model parameters. We develop an input-space technique which highlights image features that cause specific filters to malfunction to study the interaction between the image features and the erroneous filters.

2 Method

It is known that different network filters are responsible for identifying different image properties and objects [32, 31, 18, 16]. This motivates the idea that mistakes made on wrongly classified images can be understood by investigating the network parameters, rather than only the pixels, that played a role in making a decision. We develop parameter-space saliency methods geared towards identifying and analyzing neural network parameters that are responsible for making erroneous decisions. Central to our method is the use of gradient information of the loss function as a measure of parameter sensitivity and optimality of the network at a given point in image space.

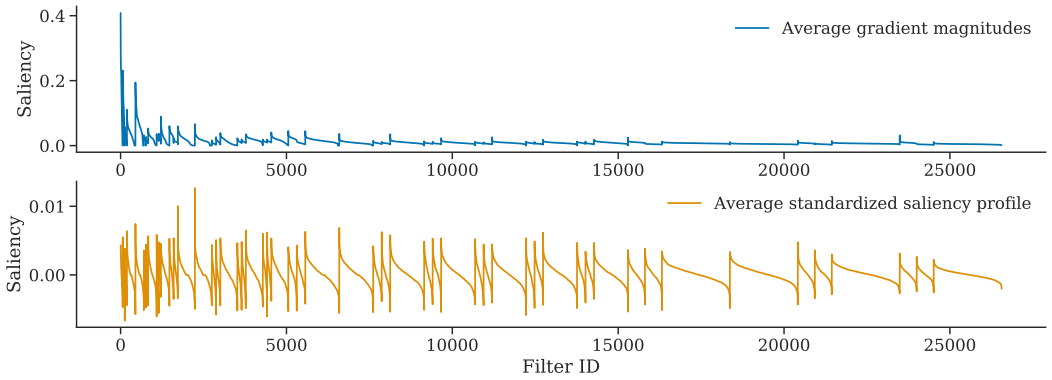

Figure 1: **Filter-wise saliency profiles.** Top: Filter-wise saliency profile (without standardization) averaged over the ImageNet validation set. Bottom: Standardized filter-wise saliency profile averaged across the ImageNet validation set. On both panels, the filter saliency values in each layer are sorted in descending order, and each layer's saliency values are concatenated. The layers are displayed left-to-right from shallow to deep. Both profiles are generated on ResNet-50.

2.1 Parameter saliency profile

Let x be a sample in the validation set D with label y, and suppose a trained classifier has parameters θ that minimize a loss function $\mathcal{L}$. We define the *parameter-wise* saliency profile of x as a vector $s(x, y)$ with entries $s(x, y)_i := |\nabla_{\theta_i} \mathcal{L}_\theta(x, y)|$, the magnitudes of the gradient of the loss with respect to each model parameter. Because the gradients on *training* data for a model trained to convergence are near zero, it is important to specify that D be a validation, or holdout, set. Intuitively, a larger gradient norm at the point (x, y) indicates a greater inefficiency in the network's classification of sample x, and thus each entry of $s(x, y)$ measures the suboptimality of individual parameters.

Aggregation of parameter saliency. Convolutional filters are known to specialize in tasks such as edge, shape, and texture detection [31, 5, 18]. We therefore choose to aggregate saliency on the filter-wise basis by averaging the gradient magnitudes of parameters corresponding to each convolutional filter. This allows us to isolate filters to which the loss is most sensitive (*i.e.* those which, when corrected, lead to the greatest reduction in loss).

Formally, for each convolutional filter $\mathcal{F}_k$ in the network, consider its corresponding index set α_k, which gives the indices of the parameters relevant to $\mathcal{F}_k$. The *filter-wise* saliency profile of x is defined to be a vector $\overline{s}(x, y)$ with entries

$$\overline{s}(x, y)_k := \frac{1}{|\alpha_k|} \sum_{i \in \alpha_k} s(x, y)_i, \tag{1}$$

the parameter-wise saliency profile aggregated by averaging on the filter level.

Standardizing parameter saliency. The top panel of Figure 1 exhibits the ResNet-50 [12] filter-wise saliency profiles averaged over the ImageNet [6] validation set, where filters within each layer are sorted from highest to lowest saliency.

One clear observation is the difference in the scale of gradient magnitudes — in the case of ResNet-50, shallower filters are more salient than deeper filters. This phenomenon might occur for a number of reasons. First, early filters encode low-level features, such as edges and textures, which are active across a wide spectrum of images. Second, typical networks have fewer filters in shallow layers than they do in deep layers, making each individual filter more influential at shallower layers. Third, the effects of early filters cascade and accumulate as they pass through a network. As a result, single early filters can be tweaked to improve performance on any given validation sample, but doing so will destroy performance on others. To isolate filters that uniquely cause *erroneous* behavior on particular samples, we find filters that are abnormally salient for a sample, x, but not for others. That is, we further standardize the saliency profile of x with respect to all filter-wise saliency profiles of D.

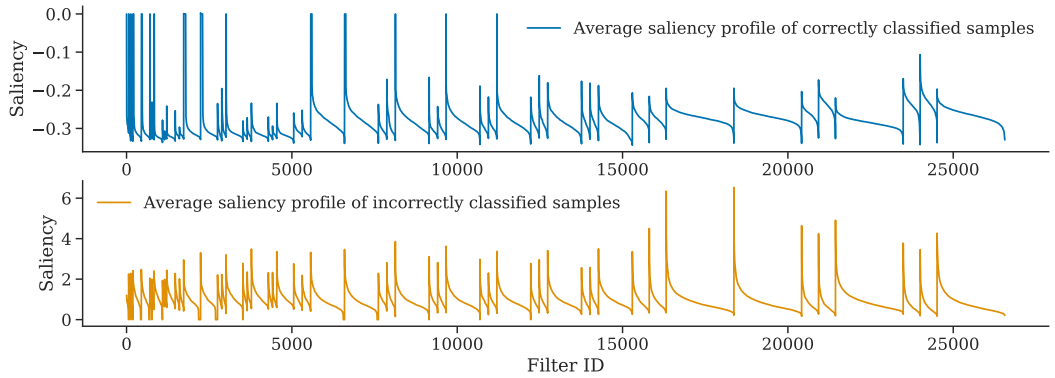

Figure 2: **Correctly vs incorrectly classified samples.** Top: Saliency profile of correctly classified samples averaged over the ImageNet validation set. Bottom: Saliency profile of incorrectly classified samples averaged over the ImageNet validation set. On both panels, the filter saliency values in each layer are sorted in descending order, and each layer's saliency values are concatenated. The layers are displayed left-to-right from shallow to deep. Both profiles are generated on ResNet-50.

Formally, let μ be the average filter-wise saliency profile across all $x \in D$, and let σ be an equal-length vector with the corresponding standard deviation for each entry. We use these statistics to produce the standardized filter-wise saliency profile as follows:

$$\hat{s}(x, y) := \frac{|\overline{s}(x, y) - \mu|}{\sigma}. \tag{2}$$

The resulting tensor $\hat{s}(x, y)$ is of length equal to the number of convolutional filters in the network, and we henceforth call it the saliency profile for sample x. By normalizing saliency profiles, we create a saliency map that activates when the importance of a filter is unusually strong relative to other samples in the dataset. This prevents the saliency map from highlighting filters that are uniformly important for all images, and instead focuses saliency on filters that are uniquely important and serve an image-dependent role. In the rest of the paper, unless explicitly noted otherwise, we use $\hat{s}(x, y)$ and refer to it as *parameter saliency*.

The bottom panel of Figure 1 presents the standardized filter-wise saliency profile averaged across the ImageNet validation set on ResNet-50. We note the improved relative scale of the saliency profile across different layers.

Incorrectly classified samples are more salient. Empirically, we observe the saliency profiles of incorrectly classified samples exhibit, on average, greater values than those of correctly classified examples. This bolsters the intuition that salient filters are precisely those malfunctioning — if the classification is correct, there should be few malfunctioning filters or none at all. Moreover, we see deeper parts of the network appear to be most salient for the incorrectly classified samples while earlier layers are often the most salient for correctly classified samples. An example of these behaviors is shown in Figure 2 for ResNet-50 averaged over the entire ImageNet validation set. Saliency profiles for other architectures could be found in Appendix A.

Henceforth, we will focus specifically on saliency profiles of *misclassified* samples in order to explore how neural networks make mistakes. We also choose to limit our study to parameter saliency profiles computed using the true label. In principle, it is possible to use a predicted label rather than the ground-truth. Computing such saliency profiles does not require the knowledge of the true label and thus could be applied to data for which the true label is unknown. As in Figure 2, we observe that on average, the profiles computed with the predicted label are more salient for the incorrectly classified samples. We refer the reader to Appendix A for more details.

2.2 Input-space saliency for visualizing how filters malfunction

The parameter saliency profile allows us to identify filters that are most responsible for mistakes and erroneous network behavior. In this section, we develop an input-space counterpart to our parameter saliency method to understand which features of the image affect the saliency of particular filters.

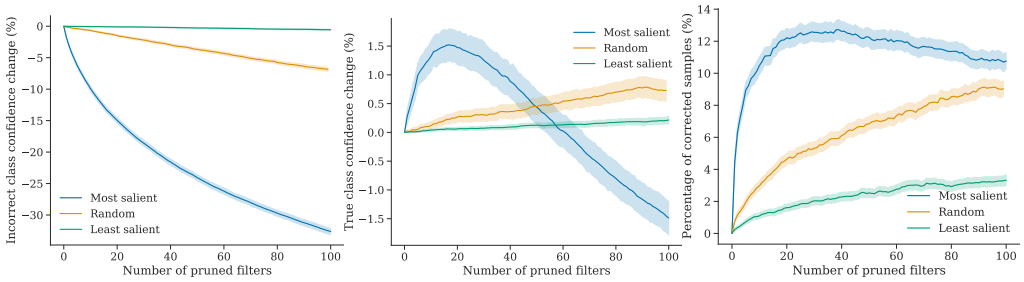

(a) (b) (c)

Figure 3: **Pruning experiments.** (a) Change in incorrect class confidence score. (b) Change in true class confidence score. (c) Percentage of samples that were corrected as the result of pruning filters. These trends are averaged across all images misclassified by ResNet-50 in the ImageNet validation set. The error bars represent 95% bootstrap confidence intervals.

Geiping et al. [11] show the gradient information of a network is invertible, providing a link between input space and parameter saliency space. This work, along with existing input-space saliency map tools [23, 25, 24, 33, 19], inspires our method.

Given a parameter saliency profile $s = s(x, y)$ for an image x with label y, our goal is to highlight the input features that cause large filter saliency values. To this end, we first select some set F of the most salient filters that we would like to explore. Then, we create a boosted saliency profile s' by increasing the entries of s corresponding to the chosen filters. Now, we can identify the input features (pixels) M_F that affect the saliency of the chosen filters F by taking the following gradients:

$$M_F = |\nabla_x D_C(s(x, y), s')|, \tag{3}$$

where $D_C(\cdot, \cdot)$ is cosine distance.

Intuitively, the components of the gradient in equation 3 with largest magnitudes represent the pixels of the original image x, whose alteration is most important for producing a new image x' with saliency profile $s(x', y)$ more closely matching s'.

3 Experiments

In this section, we aim to validate the meaningfulness of our parameter saliency method. First, we show on the dataset level that pruning the most salient filters often improves model behavior. We then find that samples which cause similar filters to malfunction are semantically similar. We also show on the dataset level that fine-tuning the most salient filters helps correct errors on other samples that are wrongly classified for similar reasons. We then use our input-space saliency technique in conjunction with its parameter-space counterpart as an explainability tool to explore how neural networks make mistakes and how salient filters interact with visual input features.

We evaluate our saliency method in the context of image classification on CIFAR-10 [14] and ImageNet [6]. Images we use for visualization, unless otherwise specified, are sampled from ImageNet validation set. Throughout the experiments, we use a pre-trained ResNet-18 classifier [12] on CIFAR-10 and a pre-trained ResNet-50 on ImageNet. Both models are trained in a standard fashion on the corresponding dataset[2][3].

3.1 Pruning salient filters

We begin validating the meaningfulness of our parameter-space saliency maps by pruning away the most salient convolutional filters (i.e. filters identified by our method as malfunctioning). In order to remove the influence of a particular salient filter, we zero out the filter weights and also the biases of

[2]https://github.com/kuangliu/pytorch-cifar (under MIT license)
[3]https://github.com/pytorch/vision (under BSD 3-Clause License)

the associated batch normalization layers. This procedure guarantees that the corresponding input feature map to the next convolutional layer is always zero.

The intuition behind this experiment is that we are trying to "switch off" the malfunctioning filters that cause misclassification on a particular image. Note that salient filters, despite causing misbehavior, may still be incredibly important for inference, and pruning is a blunt instrument for removing its influence. Thus, it is not clear that we can prune such filters without degrading performance.

Remarkably, we find that this simple procedure indeed improves the network's behavior. In particular, we gradually increase the number of pruned most salient filters and track three metrics: the change in the incorrect class confidence, the change in the true class confidence, and the percentage of the samples that flip their label to the correct class. In every case, we compare pruning the most salient filters against pruning the same number of random filters and the least salient filters. These experiments are performed on the dataset level: we average the trends across all misclassified images in the ImageNet validation set.

As shown in Figure 3, pruning the most salient filters is significantly more effective for decreasing the incorrect class confidence than random or least salient filters. Specifically, gradually pruning the top 100 salient filters achieves up to 30% drop in the incorrect class confidence score while pruning random filters yields only about 7% decrease. We also note that pruning the least salient filters does not produce any effect on the incorrect class confidence.

We repeat the same experiment with the true class confidence and observe that the highest true confidence gain occurs when we prune around 20 most salient filters. Pruning enough salient filters eventually leads to a gradual decrease in the true class confidence. We note that this behavior is expected since we are destroying, not correcting, the inference power of all of the most sensitive filters for an image, some of which may be essential for inference. Finally, pruning random filters provides a much slower increase in the true confidence class while the least salient filters again do not produce a significant effect.

In addition, we count the number of images that were corrected as a result of pruning and find that pruning around 30 most salient filters results in the best correct classification rate of 12%. Similar to the true class confidence, the trend decreases beyond this point. Pruning the random filters increases the percentage of corrected samples at a much slower rate and does not perform better than the most salient filters when pruning up to 100 filters. Notably, pruning the least salient filters manages to correct a nontrivial number of samples but still much smaller than pruning random filters.

Given the trends in panels (b) and (c) of Figure 3, and given that pruning is a coarse tool for fixing misbehavior, we explore the natural idea of correcting the most salient filters instead of removing them altogether in our fine-tuning experiments in Section 3.3.

3.2 Nearest neighbors in parameter saliency space

We validate the semantic meaning of our saliency profiles by clustering images based on the cosine similarity of their profiles. In this section, we present visual depictions of a nearest neighbor search among all images in the ImageNet validation set. We also conduct this analysis on CIFAR-10 images, and this can be found in Appendix A.

(a) Great pyrenees ↔ Kuvasz (b) Basset hound ↔ Beagle

Figure 4: **Examples of nearest neighbors in parameter saliency space (from ImageNet)**.

We find that the nearest neighbors of misclassified images in saliency space are mostly other misclassified images from the same pair of predicted and true classes but possibly in reverse order. For example, in Figure 4, the reference image in (a) is a great Pyrenees misclassified as kuvasz, and the

Figure 5: **Neighbors in saliency space found using only early or only deep layers.** The reference image is in the first column. Images in the top row resemble the reference image in the saliency on early layers of VGG-19, and images in the bottom row are found using deeper layers.

4 images with the most similar profiles exhibit either the same misclassification or the reverse (i.e., kuvasz misclassified as great Pyrenees). Intuitively, the common salient parameters across these neighbors are those which are important for discriminating between the two classes in question but are not well-tuned for this purpose.

Note that we find the concept of "being similar" in parameter saliency space to be different from the one in image space. The nearest neighbors we find are often not similar in a pixel-wise sense, but rather they are similar in their reason for causing misclassification. For example, images in Figure 4 (b) are beagles mistaken by a network for basset hounds and vice versa. We find that these pictures are either taken from a high angle or do not include the dog's legs, making the leg length, a major distinction between the two breeds, indistinguishable from the picture. We include more example images along with their nearest neighbors in Appendix A.

In addition, we compute nearest neighbors when only considering filters in a specific range of layers in order to visualize the types of misbehavior that occur at various network depths. We search for similar images using parameter saliency in the shallow and deep layers of a VGG-19 [22] network, which we divide into the shallow and deep parts that respectively occur up to and after layer `relu4_1`. The top row of figure Figure 5 shows neighbors found using shallow parameters, which share basic image attributes such as color histogram, while images in the bottom row share more abstract similarities.

3.3 Correcting mistakes by fine-tuning salient filters

To validate whether salient filters are more responsible for the erroneous behavior of neural networks, we show that updating salient filters alone is sufficient for correcting the mistakes made by a neural network. In this experiment, for a pre-trained image classification network, we fine-tune it for one step on a single image for which the network makes the wrong prediction. We restrict the number of tunable filters to be no more than 1.0% of the total number of filters in a network, and we update the chosen filters by taking one step of gradient descent with a fixed step size. To validate the effectiveness of optimizing salient filters, we compare it with two other choices of tunable filters: the least salient filters and random filters. For a more general evaluation, we use images from the ImageNet validation set that are mis-classified by a ResNet-50, making up to over 10,000 samples. We evaluate the effect of fine-tuning on each of these images independently.

In Figure 6, we compare the average performance of our three choices of tunable filters under three evaluation metrics. For a given sample image and a set of tunable filters, an update step is considered to be effective if the updated network corrects its mistake on the sample image. In addition, it is more useful if the updated network also corrects its mistake on other images that resemble the sample image but are seen during fine-tuning.

First, by inspecting the percentage of samples that are corrected after undergoing fine-tuning, we find that updating 150 salient filters ($\sim$0.6% of total filters) can achieve the same result as updating the entire network. The second and the third evaluation measure the effect on the nearest neighbors of the training sample. We find nearest neighbors for each training sample through the process introduced in Section 3.2, where we limit the search scope exclusively to other misclassified images. Note that for a given training sample, its nearest neighbors are not involved in our one-step single sample fine-tuning process. By tracking model predictions and true class confidence scores among the 10

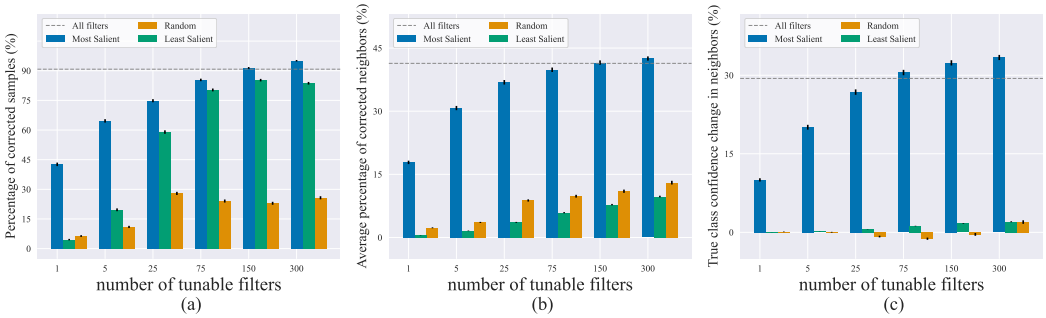

Figure 6: **Effect of updating a small number of filters.** (a) Percentage of samples that are corrected after fine-tuning. (b) Average percentage of nearest neighbors that are also corrected after fine-tuning. (c) Average change in the confidence score of the true class among nearest neighbors. The horizontal line in each plot is the effect of updating the entire network.

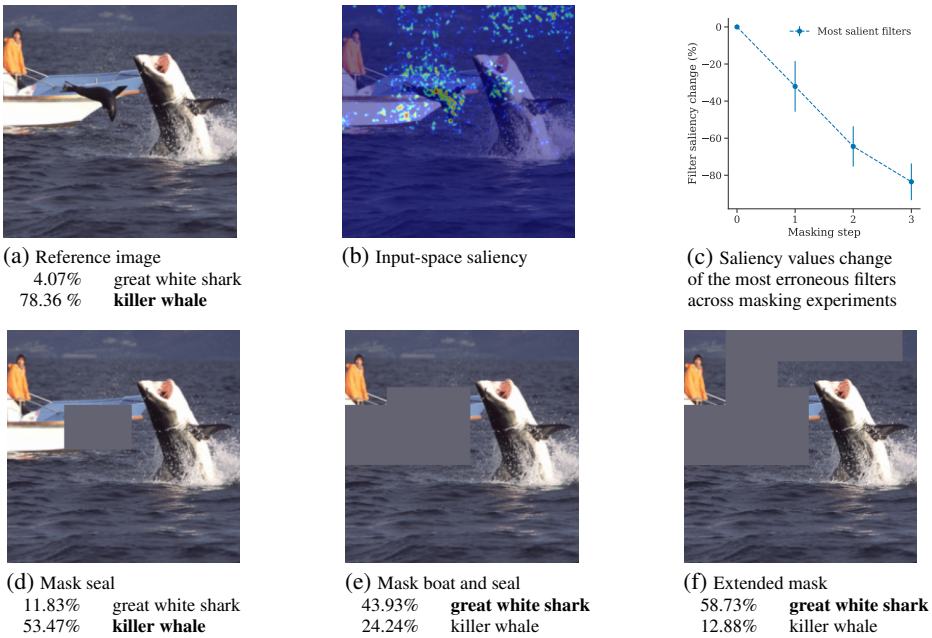

(a) Reference image
4.07% great white shark
78.36 % **killer whale**

(b) Input-space saliency

(c) Saliency values change of the most erroneous filters across masking experiments

(d) Mask seal
11.83% great white shark
53.47% **killer whale**

(e) Mask boat and seal
43.93% **great white shark**
24.24% killer whale

(f) Extended mask
58.73% **great white shark**
12.88% killer whale

Figure 7: **Interaction between input features and salient filters.** (a) Reference image of "great white shark" misclassified by ResNet-50 as "killer whale" with confidence scores. (b) Input-space saliency visualization. Pixels that cause the top 10 salient filters to have high saliency. (c) Change in saliency values of the erroneous filters across masking experiments. The vertical bars represent the standard deviation of the change across 10 most salient filters. (d)-(f) Masking experiments.

nearest neighbors of each sample, we find that fine-tuning salient filters is significantly more effective than other choices. Results in Figure 6, (b) and (c), also imply that the nearest neighbors found using our method are the images that are wrong for similar reasons and that they can be corrected altogether by only updating the salient filters.

3.4 Input features that cause filters to malfunction: a case study

We consider the case study of an image misclassified by ResNet-50 as "killer whale" (Figure 7(a)). The correct label of the image is "great white shark". Our goal is to study the interaction between the most salient filters and input features. We first identify filters most responsible for misclassification by computing the saliency profile and visualize parts of the image that drive the high saliency values for those filters using our input-space saliency technique (Section 2.2).

Panel (b) of Figure 7 presents our image-space visualization, which depicts the causes of misbehavior for the ten most salient filters – the pixels that trigger misbehavior in these filters are highlighted. For example, we see that the seal and boat are both triggers. One natural hypothesis is that the seal looks like a killer whale to the network and is the source of the classification error. We test this hypothesis by masking out the seal (Figure 7 (d)) . However, although the probability of "killer whale" goes down and the probablity of the correct class increases, the network still misclassifies the image as "killer whale".

Now, if we mask out exactly the most salient areas of the image according to our visualization (see Figure 7 (b), (e)), the network manages to flip the label of the image and classify it correctly. If we extend our mask to the less pronounced, but still salient, areas of the image as in Figure 7 (f), we observe that the correct class confidence increases even more while the probability of the incorrect "killer whale" label further decreases. Additionally, we find that masking out the non-salient parts of the image results in even worse misclassification confidence than that of the original image (see Appendix A). In order to further investigate the effect of the salient region, we pasted it from this image onto other great white shark images (see Appendix A) and observed that this drives the probability of "killer whale" up for 39 out of 40 examples of great white sharks from the ImageNet validation set with an average increase of 3.75%.

Our experiments suggest that secondary objects in the image are associated with the misclassification. However, we see that the erroneous behavior of the model does not just stem from classifying a non-target object in the image. It is possible that the model correlates the combination of sea creatures (e.g. a seal) and man-made structures (e.g. a boat) with the "killer whale" label. We note that images of killer whales in ImageNet often have man-made structures which look similar to the boat (see Appendix A for examples of other "killer whale" images).

Finally, at each step of our masking experiments, we recompute the saliency values of the originally chosen 10 filters (i.e. the filters that caused erroneous behavior on the reference image). From Figure 7 (c), we observe that as we mask out the input features according to our input-saliency, the saliency values of those filters decrease gradually and reach an 80% drop, confirming that highlighted regions indeed drive the high saliency of the chosen filters.

More visualizations of input space saliency showcasing different illustrative examples of neural network mistakes can be found in Figure 8. For a thorough discussion of mistake categories we identify using our saliency method, we refer to Appendix A.

4 Discussion

Numerous applications demand that practitioners be able to understand the decisions their models make, especially when those decisions are incorrect. Existing methods for explainability focus on locating the input regions to which the network's output is sensitive or on associating network components with specific roles. In contrast, we develop a framework for finding the exact filters which are responsible for faulty predictions and studying the interactions between these filters and images. This direction yields both an interpretable and intuitive understanding of model behaviors.

5 Limitations and Impact

Although our formulation of parameter saliency is not restricted to image datasets and CNNs, we only conduct experiments in these settings. In contrast, real-world data and models come in many forms. Explainability methods which shed light in some settings may fail to do so in others. Moreover, we emphasize that some erroneous model behaviors are simply difficult to understand through existing methods, and the capabilities of parameter saliency are limited. In many applications, it is imperative that practitioners understand why their models behave as they do and that they are able to diagnose problems when they arise. We hope that our work helps to enable solutions to real-world problems. However, we caution against a false sense of security. Our visual interpretations of model behavior should be viewed as approximations as neural networks are incredibly complex.

(a) dalmation / soccer ball (b) pizza / bell pepper (c) leopard / jaguar (d) junco / house finch (e) passenger car / locomotive

Figure 8: **Different types of network mistakes.** All of the presented images are misclassified by ResNet-50. The correct class label is specified in the top row and the incorrect class label – in the bottom row of the subcaption on each panel. (a)-(b) The target object is confused with another object in the image. (c) A regular mistake. The salient pixels are focused on the target object features which confuse the network. (d) Background features confuse the network. (e) An example of a noisy label where the network is "more correct" than the target label. These are examples where masking top 5% of the salient pixels corrects the misclassification.

6 Acknowledgements

This work was supported by the DARPA YFA program, DARPA GARD, the ONR MURI program, the National Science Foundations Division of Mathematical Sciences, the AFOSR MURI program, and Capital One Bank.

References

[1] R. Abbasi-Asl and B. Yu. Interpreting convolutional neural networks through compression. *arXiv preprint arXiv:1711.02329*, 2017.

[2] J. Adebayo, J. Gilmer, M. Muelly, I. Goodfellow, M. Hardt, and B. Kim. Sanity checks for saliency maps. *arXiv preprint arXiv:1810.03292*, 2018.

[3] A. Alqaraawi, M. Schuessler, P. Weiß, E. Costanza, and N. Berthouze. Evaluating saliency map explanations for convolutional neural networks: a user study. In *Proceedings of the 25th International Conference on Intelligent User Interfaces*, pages 275–285, 2020.

[4] A. Bau, Y. Belinkov, H. Sajjad, N. Durrani, F. Dalvi, and J. Glass. Identifying and controlling important neurons in neural machine translation. *arXiv preprint arXiv:1811.01157*, 2018.

[5] D. Bau, B. Zhou, A. Khosla, A. Oliva, and A. Torralba. Network dissection: Quantifying interpretability of deep visual representations. In *Proceedings of the IEEE conference on computer vision and pattern recognition*, pages 6541–6549, 2017.

[6] J. Deng, W. Dong, R. Socher, L.-J. Li, K. Li, and L. Fei-Fei. ImageNet: A Large-Scale Hierarchical Image Database. In *CVPR09*, 2009.

[7] J. Deng, J. Guo, N. Xue, and S. Zafeiriou. Arcface: Additive angular margin loss for deep face recognition. In *Proceedings of the IEEE/CVF Conference on Computer Vision and Pattern Recognition*, pages 4690–4699, 2019.

[8] D. Erhan, Y. Bengio, A. Courville, and P. Vincent. Visualizing higher-layer features of a deep network. *University of Montreal*, 1341(3):1, 2009.

[9] European Commission. *Recital 71 EU General Data Protection Regulation*. 2018. URL `https://www.privacy-regulation.eu/en/r71.htm`.

[10] R. C. Fong and A. Vedaldi. Interpretable explanations of black boxes by meaningful perturbation. In *ICCV*, 2017.

[11] J. Geiping, H. Bauermeister, H. Dröge, and M. Moeller. Inverting gradients–how easy is it to break privacy in federated learning? *arXiv preprint arXiv:2003.14053*, 2020.

[12] K. He, X. Zhang, S. Ren, and J. Sun. Deep residual learning for image recognition. In *CVPR*, 2016.

[13] E. Kang, J. Min, and J. C. Ye. A deep convolutional neural network using directional wavelets for low-dose x-ray ct reconstruction. *Medical physics*, 44(10):e360–e375, 2017.

[14] A. Krizhevsky. Learning multiple layers of features from tiny images. Technical report, 2009.

[15] C. Liu and H. Wu. Channel pruning based on mean gradient for accelerating convolutional neural networks. *Signal Processing*, 156:84–91, 2019.

[16] A. Mahendran and A. Vedaldi. Understanding deep image representations by inverting them. In *CVPR*, 2015.

[17] A. S. Morcos, D. G. Barrett, N. C. Rabinowitz, and M. Botvinick. On the importance of single directions for generalization. *arXiv preprint arXiv:1803.06959*, 2018.

[18] C. Olah, A. Mordvintsev, and L. Schubert. Feature visualization. *Distill*, 2017. doi: 10.23915/distill.00007. https://distill.pub/2017/feature-visualization.

[19] R. R. Selvaraju, M. Cogswell, A. Das, R. Vedantam, D. Parikh, and D. Batra. Grad-cam: Visual explanations from deep networks via gradient-based localization. In *ICCV*, 2017.

[20] A. Shrikumar, P. Greenside, A. Shcherbina, and A. Kundaje. Not just a black box: Learning important features through propagating activation differences. 2016. *arXiv preprint arXiv:1605.01713*.

[21] A. Shrikumar, P. Greenside, and A. Kundaje. Learning important features through propagating activation differences. In *ICML*, 2017.

[22] K. Simonyan and A. Zisserman. Very deep convolutional networks for large-scale image recognition. In *ICLR*, 2015.

[23] K. Simonyan, A. Vedaldi, and A. Zisserman. Deep inside convolutional networks: Visualising image classification models and saliency maps. In *ICLR*, 2014.

[24] D. Smilkov, N. Thorat, B. Kim, F. Viégas, and M. Wattenberg. Smoothgrad: removing noise by adding noise. *arXiv preprint arXiv:1706.03825*, 2017.

[25] J. T. Springenberg, A. Dosovitskiy, T. Brox, and M. Riedmiller. Striving for simplicity: The all convolutional net. In *ICLR*, 2015.

[26] S. Srinivas and F. Fleuret. Full-gradient representation for neural network visualization. *arXiv preprint arXiv:1905.00780*, 2019.

[27] M. Sundararajan, A. Taly, and Q. Yan. Axiomatic attribution for deep networks. In *ICML*, 2017.

[28] United States Congress Senate Committee on Banking and Housing and Urban Affairs. *Equal Credit Opportunity Act. [electronic resource].* S. Rpt. 94-685. Washington, 1976.

[29] H. Wang, Z. Wang, M. Du, F. Yang, Z. Zhang, S. Ding, P. Mardziel, and X. Hu. Score-cam: Score-weighted visual explanations for convolutional neural networks. In *CVPR*, 2020.

[30] D. West. Neural network credit scoring models. *Computers & Operations Research*, 27(11-12): 1131–1152, 2000.

[31] J. Yosinski, J. Clune, A. Nguyen, T. Fuchs, and H. Lipson. Understanding neural networks through deep visualization. *arXiv preprint arXiv:1506.06579*, 2015.

[32] M. D. Zeiler and R. Fergus. Visualizing and understanding convolutional networks. In *European conference on computer vision*, pages 818–833. Springer, 2014.

[33] B. Zhou, A. Khosla, A. Lapedriza, A. Oliva, and A. Torralba. Learning deep features for discriminative localization. In *Proceedings of the IEEE conference on computer vision and pattern recognition*, pages 2921–2929, 2016.

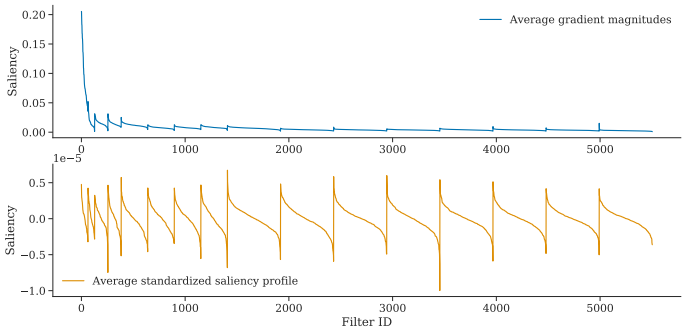

(a) VGG-19

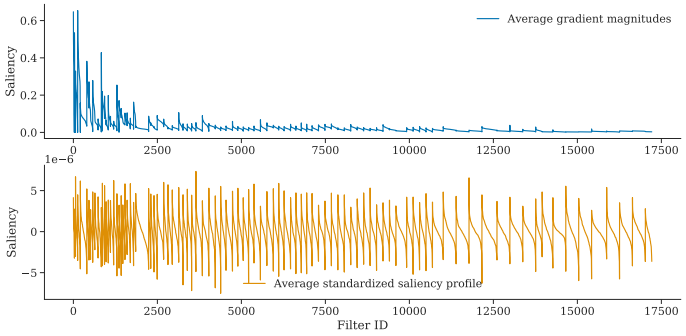

(b) Inception v3

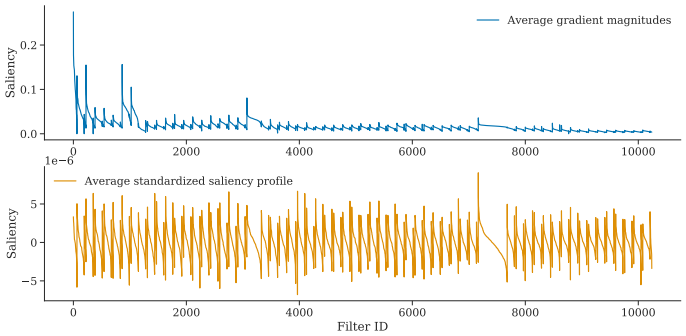

(c) DenseNet

Figure 9: **Filter-wise saliency profiles for other architectures.** (a) VGG-19 saliency profiles. (b) Inception v3 saliency profiles. (c) DenseNet saliency profiles. In each panel, the top row presents filter-wise saliency profile (without standardization) averaged over the ImageNet validation set and the bottom row shows standardized filter-wise saliency profile averaged across the ImageNet validation set. In every panel, the filter saliency values in each layer are sorted in descending order, and each layer's saliency values are concatenated. The layers are displayed left-to-right from shallow to deep.

A Additional Experiments

A.1 Parameter saliency profiles for other network architectures

In this section, we present average saliency profiles for several popular network architectures other than ResNet-50 [12]. Analogously to Figure 1, Figure 9 presents average gradient magnitudes vs average standardized saliency profiles for VGG-19 [22], Inception v3 [35], and DenseNet [34]. Similarly to Figure 2, we also present in Figure 10 standardized filter-wise saliency profiles for those architectures averaged across correctly and incorrectly classified ImageNet [6] samples.

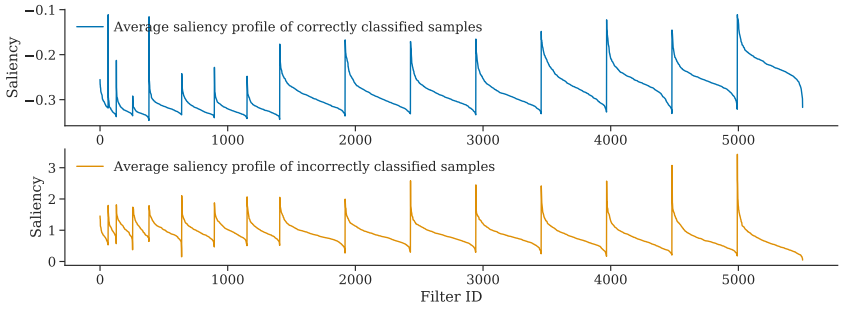

(a) VGG-19

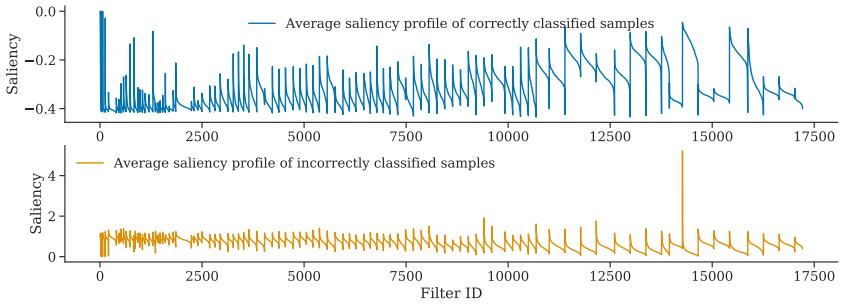

(b) Inception v3

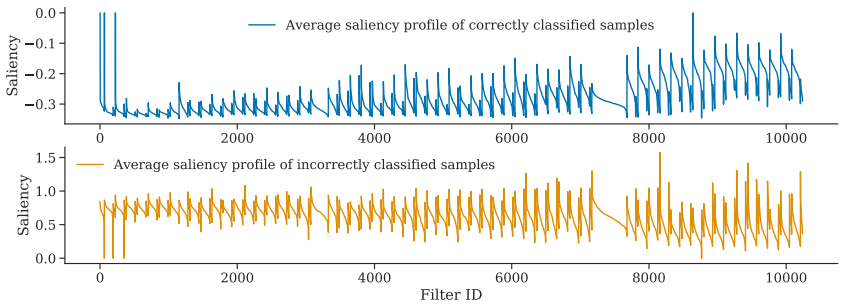

(c) DenseNet

Figure 10: **Average saliency profiles across correctly vs incorrectly classified samples.** (a) VGG-19 saliency profiles. (b) Inception v3 saliency profiles. (c) DenseNet saliency profiles. In each panel, the top row presents the saliency profiles of correctly classified samples averaged over the ImageNet validation set and the bottom row shows saliency profiles of incorrectly classified samples averaged over the ImageNet validation set. On every panel, the filter saliency values in each layer are sorted in descending order, and each layer's saliency values are concatenated. The layers are displayed left-to-right from shallow to deep.

A.2 Parameter saliency profiles with predicted label

As discussed in section 2.1, it is possible to use a predicted label rather than the ground-truth. Computing such saliency profiles does not require the knowledge of the true label and thus could be applied to data for which the true label is unknown. As Figure 11 shows, we observe that on average the saliency profiles computed with the predicted label are more salient for the incorrectly classified samples than for correctly classified samples. However, we also note that the average saliency values computed with the predicted label are lower for the incorrectly classified samples than the average saliency values of those samples computed with the ground-truth label (the saliency profiles for the ground-truth label are presented in Figure 2).

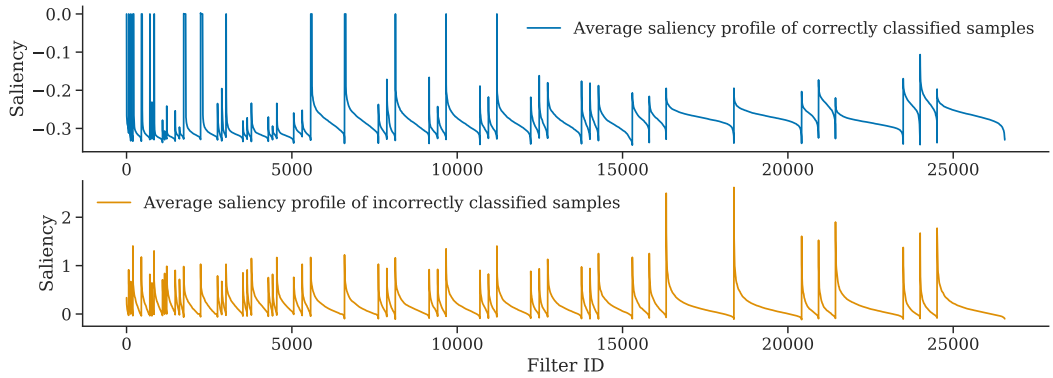

Figure 11: **Saliency profiles computed with predicted label. Correctly vs incorrectly classified samples.** Top: Saliency profile of correctly classified samples averaged over the ImageNet validation set. Bottom: Saliency profile of incorrectly classified samples averaged over the ImageNet validation set. On both panels, the filter saliency values in each layer are sorted in descending order, and each layer's saliency values are concatenated. The layers are displayed left-to-right from shallow to deep. Both profiles are generated on ResNet-50.

A.3 More examples of nearest neighbors

We present more examples of nearest neighbors in our parameter saliency space. Figure 12 are nearest neighbors in CIFAR-10 [14] dataset, where reference images are chosen from samples misclassified by our classifier. Figure 13 are examples from ImageNet, where images are captioned with the true label of the reference images.

(a) bird ↔ cat (b) frog ↔ cat (c) airplane ↔ ship (d) horse ↔ deer

Figure 12: **CIFAR-10 examples of nearest neighbors in parameter saliency space**. On CIFAR-10 images that cause similar filters to malfunction are often misclassified in a similar way.

(a) coyote (b) goldfish (c) terrapin (d) great white shark

Figure 13: **ImageNet examples of nearest neighbors in parameter saliency space**. In every panel, the reference image is in the left column and its nearest neighbors are in the right column. Panels are captioned by the true label of their reference image.

A.4 Fine-tuning salient filters of a VGG-19

In this section, we conduct the fine-tuning experiment introduced in Section 3.3 on a VGG-19 network trained on ImageNet, which has a total of 5504 filters. The learning rate for training our VGG network is 1/10 of that for the ResNet, so we decrease the fine-tuning step size by 10 in this experiment. Figure 14 shows the effect of updating salient filters of a VGG-19. Note that we use the same range for the number of tunable filters in this experiment; 300 filters correspond to 5.5% of total filters in a VGG-19, while it is 1.2% for a ResNet-50.

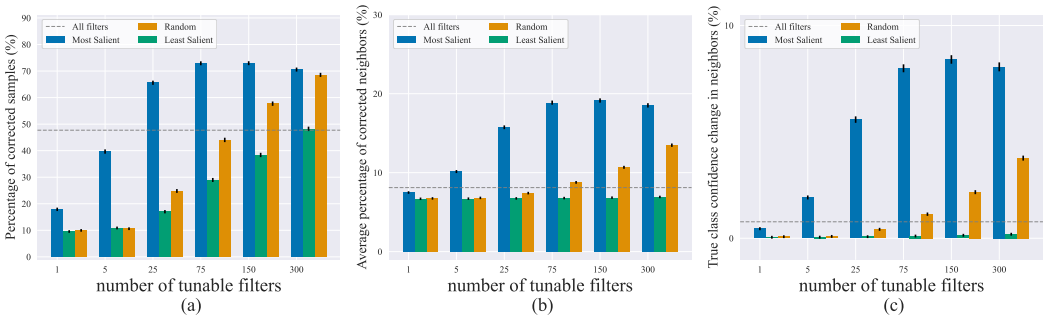

Figure 14: **Effect of updating a small number of filters on VGG-19.** (a) Percentage of samples that are corrected after fine-tuning. (b) Average percentage of nearest neighbors that are also corrected after fine-tuning. (c) Average change in the confidence score of the true class among nearest neighbors. The horizontal line in each plot is the effect of updating the entire network.

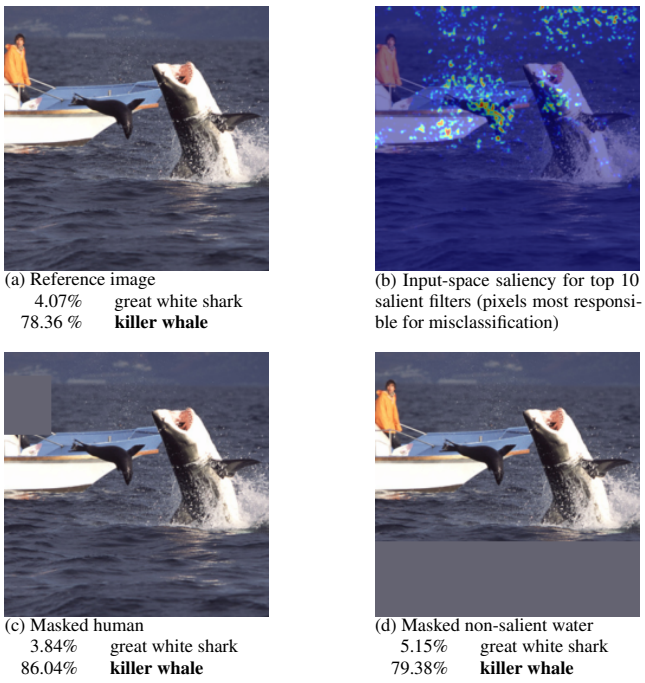

(a) Reference image
4.07% great white shark
78.36 % **killer whale**

(b) Input-space saliency for top 10 salient filters (pixels most responsible for misclassification)

(c) Masked human
3.84% great white shark
86.04% **killer whale**

(d) Masked non-salient water
5.15% great white shark
79.38% **killer whale**

Figure 15: **Masking non-salient parts of the image.** (a) Reference image of “great white shark" misclassified by the model as “killer whale" and the corresponding confidence scores. (b) Pixels that cause the top 10 most salient filters to have high saliency. (c) Masked (non-salient) human. (d) Masked non-salient water region.

A.5 Additional case study figures

Masking non-salient parts of the image. As noted in section 3.4 and presented in Figure 15, masking the non-salient parts of the image results in even worse misclassification confidence with the incorrect class confidence increasing compared to the reference image.

Pasting the salient region from the reference image onto other “great white shark" images. As mentioned in section 3.4, in order to further investigate the effect of the salient region, we pasted it (i.e., the seal and the boat) from the original image onto other images with “great white shark" ground truth label that were correctly classified by ResNet-50 (see Figure 16 for examples). We observed that this increased the probability of “killer whale” for 39 out of 40 examples of great white sharks from the ImageNet validation set with an average increase of 3.75%.

Examples of images with “killer whale" label. As we discussed in section 3.4, the model might have learned to correlate a combination of sea creatures (e.g. a seal) and man-made structures (e.g. a boat) with the “killer whale” label. Images of killer whales in ImageNet often have man-made structures which look similar to the boat, we provide examples of that in Figure 17.

Figure 16: **Sample “great white shark" images with boat and seal.** The salient region from the case study image pasted onto other “great white shark" images.

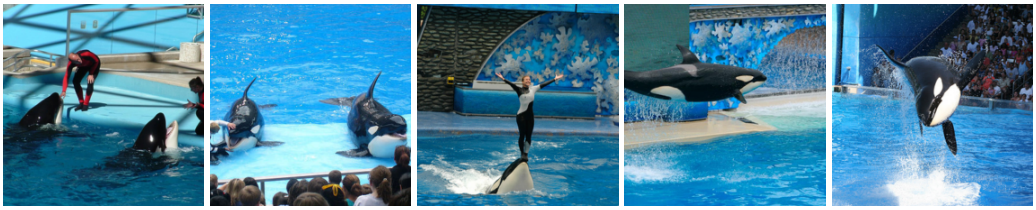

Figure 17: **ImageNet examples of “killer whale".**

A.6 Exploring neural network mistakes

In Section 3.4, we apply our parameter-space saliency method as an explainability tool using it alongside our input-space technique to study how image features cause specific filters to malfunction. In our case study, the salient pixels that confuse the network are focused less on the target object than on other image features, and masking the salient regions which are not on the target object improves the network behavior. Such examples expose the network’s reliance on spurious correlations and constitute an interesting type of model mistake.

The masking approach can be adopted to explore network mistakes and find other interesting cases (e.g., cases where the salient pixels are not concentrated on the target object). Investigating examples where masking the most salient pixels improves performance may provide insights into the model’s misbehavior as well as expose dataset noise and biases. We select misclassified samples where masking the top 5% of salient pixels leads to an increase of at least 25% in confidence corresponding to the correct class. We showcase representative examples of different types of mistakes that we observe in those samples in Figure 8. Many of the neural network misclassifications stem from classifying a non-target object in images with multiple objects (see Figure 8 (a), (b)). However, other mistakes are triggered by background features (Figure 8 (d)), dataset biases (as our case study experiments in Figure 7 suggest), and label noise (Figure 8 (e)).

Interestingly, in some of the selected cases the salient regions still focus on the target object features (see Figure 8 (c)), and masking them improves the model’s behavior. Masking salient target object features that confuse the network seems to be particularly beneficial for images of animals; for example, masking dog ears helps the network identify the correct breed (see Figure 18(a)) or masking spot patterns helps distinguish different types of rays (see Figure 18(b)).

While masking the top 5 % of salient pixels results in correct classification for all samples in Figure 8 and in Figure 18(a), (b), this is, of course, not always the case. Sometimes, pixels which cause large filter saliency values are focused densely on the target object, and masking them results in decreased confidence corresponding to the correct class. Selecting such samples can be used to find situations where the network is genuinely confused by the target object rather than background features (Figure 18 (c)) or samples with multiple objects present and with salient pixels more focused on the target object (Figure 18 (d)).

Figure 18: **Pixels responsible for mistakes focused on the target object.** (a)-(b) Masking the salient pixels corrects the misclassification where masking confusing features (e.g. dog ears or spot patterns) helps distinguish animals. (c)-(d) Masking the salient pixels results in correct class confidence decrease, when the salient pixels are densely focused on the target object. The correct class label is specified in the top row and the predicted incorrect class label – in the bottom row of the subcaption on each panel.

A.7 Comparison to GradCAM

As we mention in Section 1.1, existing input saliency maps used with the predicted label can highlight features which are related to misclassification. However, they are not specifically geared towards that goal. Our input saliency technique highlights image features that cause specific filters to malfunction and those features, while they might in some cases coincide with the features that explain a high class confidence score corresponding to the predicted label, may not be the same.

In this section, we will compare our input-space saliency technique which highlights pixels that drive high parameter saliency values of specific filters (i.e., pixels that confuse the network) to the visual explanations produced by GradCAM with the predicted label [4] [19] – one of the most popular and high quality input-saliency methods.

Figures 19 and 20 present panels of images comparing our method to GradCAM explanations computed with the predicted label. From the perspective of highlighting pixels responsible for neural network mistakes and for driving high filter saliency values, we note the following:

- GradCAM highlights the object that corresponds to the incorrect label, and the entire target object is highlighted in the images where only the target object is present (see Figure 19 (c)-(e), Figure 20 (a)-(c)). However, when our method focuses on the target object, it highlights specific features of that object. Those are the features that confuse the network, and masking them can correct the misclassification.
- In cases where the network classifies the non-target object in the image (see Figure 19 (a)-(b), Figure 20 (d)), both methods highlight the non-target objects. However, GradCAM is more localized to the non-target object. This is expected since GradCAM produces visual explanations for the predicted label (and has been shown to produce highly localized saliency maps [19]) while our method highlights all pixels that drive the filter saliency, and these pixels may be located on the target object as well.
- In cases where the misclassification does not stem from confusion by the target object or classifying the non-target object (see Figure 19 (d)-(e), Figure 20 (e)), our method highlights background features and/or a combination of non-target object features, while GradCAM still highlights the target object. For example, in Figure 20 (e), our method highlights the

[4] Implementation from https://github.com/kazuto1011/grad-cam-pytorch under MIT license

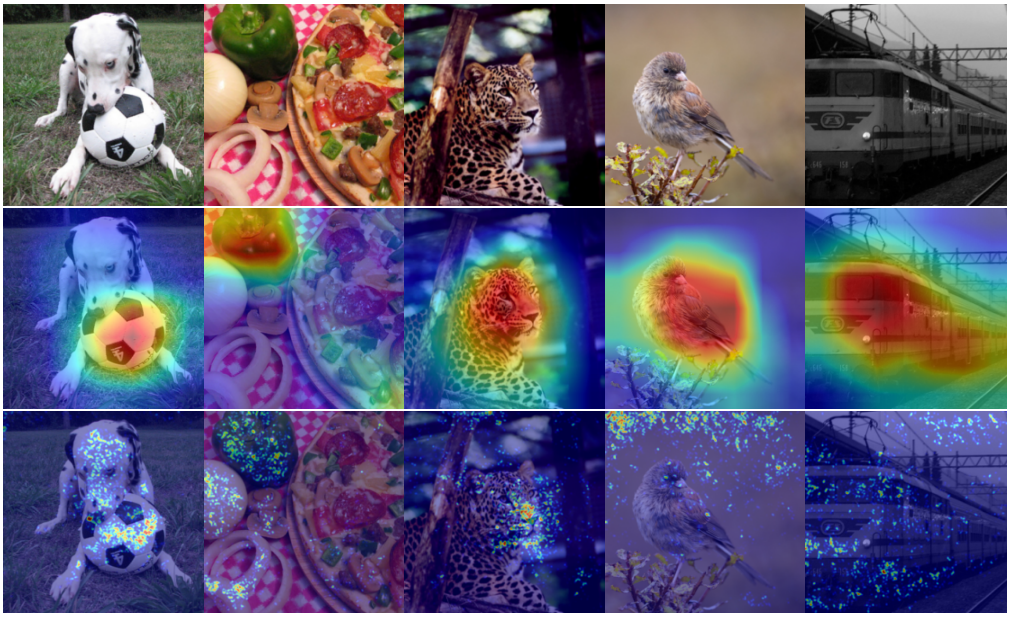

Figure 19: **Comparison to GradCAM.** Top row: original image. Middle row: GradCAM input-space saliency map for the predicted label. Bottom row: our input-space saliency technique which highlights pixels that drive high parameter saliency values of specific filters (i.e., pixels that confuse the network). The correct class label is specified in the top row and the predicted incorrect class label – in the bottom row of the subcaption on each panel.

boat and the sky much more than GradCAM, and our case study masking experiments in section 3.4 show that those regions indeed confuse the network.

- In addition, we emphasize that our input saliency technique is specific to the chosen filter set F and is introduced to study the interaction between the image features and the malfunctioning filters. In contrast, GradCAM is not able to relate image-space mistakes to an arbitrary set of model parameters or filters chosen by the user.

To summarize, GradCAM (as well as many other input-space saliency methods) was designed to be highly localized to the object correponding to the label of interest, while our method highlights sparse fine-grained features of images which we believe is a desirable property for our specific application. Therefore, we opt for using input-gradient information similar to the original Vanilla Gradient [23] method. However, instead of class confidence scores, we use a different loss – cosine distance to the boosted parameter-saliency profile (as described in Section 2.2) which allows us to explore how image features cause specific filters to malfunction.

A.8 Input-saliency sanity check

To assure that our input-space saliency technique is model dependent, we performed the model randomization test from [2]. We can see that the input saliency map is model dependent. We note that the data randomization test is not applicable in our case because our input-space saliency map is based on the parameter-saliency profile and parameter-saliency is designed to investigate a pretrained model with particular weights.

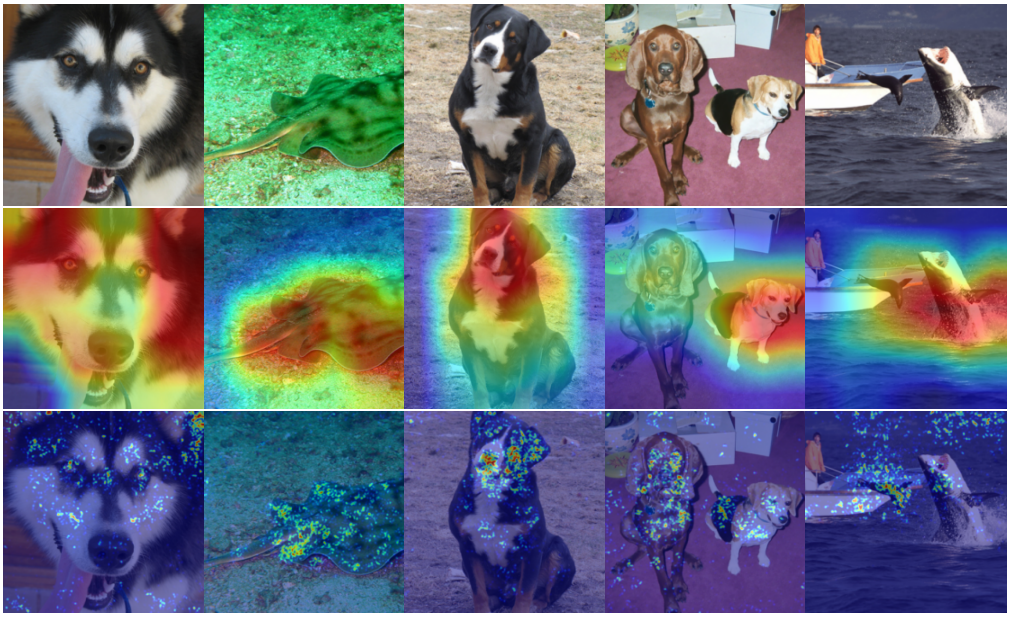

(a) malamute husky (b) stingray electric ray (c) appenzeller sennenhund (d) redbone beagle (e) great white shark killer whale

Figure 20: **Comparison to GradCAM.** Top row: original image. Middle row: GradCAM input-space saliency map for the predicted label. Bottom row: our input-space saliency technique which highlights pixels that drive high parameter saliency values of specific filters (i.e., pixels that confuse the network). The correct class label is specified in the top row and the predicted incorrect class label – in the bottom row of the subcaption on each panel.

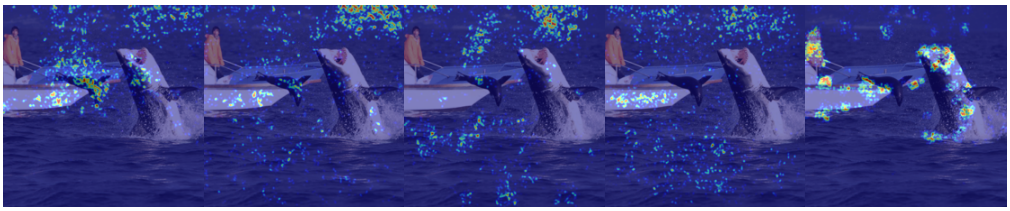

(a) Original (b) Stage 4 (c) Stages 3-4 (d) Stages 2-4 (e) Stages 1-4

Figure 21: **Sanity checks.**(a) No randomization of ResNet-50. (b) Only stage 4 of ResNet-50 is randomized. (c) Stages 3-4 of ResNet-50 are randomized. (d) Stages 2-4 of ResNet-50 are randomized. (e) The entire ResNet-50 is randomized.

B Implementation details

B.1 Hyper-parameter setting for fine-tuning salient filters

When tuning a small number of random or least salient filters, we re-normalize the gradient magnitude of these parameters to be the same as the salient filters for a fair comparison; otherwise the gradients for these parameters are always smaller than the salient ones by the definition of our saliency profile, and updating them would make less change to a model than updating the salient ones. In addition to re-normalizing the gradients, we also multiply them with a step size, similar to the concept of learning rate in stochastic gradient descent. For ResNet-50, we set the step size to be 0.001, which equals to the learning rate of the last epoch when training the ResNet-50 on ImageNet from scratch. For VGG-19, we also set the fine-tuning step size to be the learning rate from the last training epoch, which is 0.0001.

B.2 Input saliency visualization

The number of top salient filters to boost was chosen to be 10 in all input-space saliency experiments. The filters were boosted by multiplying by 100. For visualization, absolute input gradients were thresholded at 90-th percentile and Gaussian Blur with $(3, 3)$ kernel was applied.

B.3 Hardware

The experiments were run on Nvidia GeForce RTX 2080Ti GPUs with 11Gb GPU memory on a machine with 4 cpu cores and 64Gb RAM. The input-space and parameter-saliency profiles take seconds to compute for a single sample.

Additional References

[34] G. Huang, Z. Liu, L. Van Der Maaten, and K. Q. Weinberger. Densely connected convolutional networks. In *Proceedings of the IEEE conference on computer vision and pattern recognition*, pages 4700–4708, 2017.

[35] C. Szegedy, V. Vanhoucke, S. Ioffe, J. Shlens, and Z. Wojna. Rethinking the inception architecture for computer vision. In *Proceedings of the IEEE conference on computer vision and pattern recognition*, pages 2818–2826, 2016.